Available online at www.sciencedirect.com
ScienceDirect
Journal of Sound and Vibration 305 (2007) 243–260
JOURNAL OF SOUND AND VIBRATION
www.elsevier.com/locate/jsvi

Investigation of the effects of air on the dynamic behavior of a small cantilever beam

H. Nouira[a,*], E. Foltête[a], L. Hirsinger[a], S. Ballandras[b]

[a]Department of Applied Mechanics, FEMTO-ST Institute, 24 Chemin de l'Epitaphe, 25000 Besançon, France
[b]Department of Physics and Metrology of Oscillator, FEMTO-ST Institute, 32 Avenue de l'Observatoire, 25044 Besançon, France

Received 24 July 2006; received in revised form 28 March 2007; accepted 2 April 2007

Abstract

There has been a growing interest these past years in microsystems and understanding the mechanical properties essential for their design. In this context, an experimental technique is proposed to characterize a small dimensional structure surrounded by various air pressure levels. Dynamic tests were performed on three different cantilever beams (silicon single-crystal, quartz and lithium niobate) used in the realization of an energy converter. The beam is mounted on a support and excited by a shaker. The dynamic responses recorded by a laser vibrometer allow the corresponding modal parameters to be identified as a function of the air pressure inside the vacuum chamber. A nonlinear modal identification is then performed. It is based on the logarithmic decrement method applied in the time–frequency domain using a wavelet transform of the time responses. The evolution of the equivalent modal frequency and the equivalent modal damping of the beam versus time and vibration amplitude are identified for several pressure values ranging from a primary vacuum to atmospheric pressure. Finally, an analytical simulation with the Hosaka theoretical model is presented. Comparing this theoretical model with experimental results, a good agreement was obtained for silicon structure.

1. Introduction

In the context of the design and the manufacturing of a microconverter, whose role is to transform the ambient vibratory mechanical energy into electrical power, an investigation into the effects of air on the dynamic behavior of a small cantilever beam has been performed. To ensure an affective conversion, the energy losses must be minimized. The objective of this study is to quantify, by different techniques, the damping due to the surrounding media and its influence on the structure's dynamic behavior. The damping study is very important during the development of mechanical microsystems, since it directly influences their dynamic performance. The energy dissipation due to internal friction has been analyzed using the structural damping theory described by Avallone [1]. The elastic energy dissipation in the clamped end is classified among the most significant sources because the contact interfaces are never perfectly smooth. Jimbo and Ito [2] provided a closed-form solution for the energy dissipation in an elastic foundation based on

*Corresponding author. Fax: +33 3 81 66 67 00.
E-mail address: hichem.nouira@univ-fcomte.fr (H. Nouira).

0022-460X/$ - see front matter © 2007 Elsevier Ltd. All rights reserved.
doi:10.1016/j.jsv.2007.04.013

two-dimensional (2D) elasticity theory. In microsystems, other dissipation sources occur such as airflow damping caused by the contact of the structure with the open air, or squeeze damping caused by the contact of vibratory structure with confined air, and of course damping due to acoustic radiation of the device in the surrounding media if the structure is not enclosed. The presence of air around a vibrating structure produces viscous damping that was estimated analytically by Tarasawa et al. [3]. Blom et al. [4] analytically obtained the damping ratio of a vacuum gauge resonator by modeling the resonator as a string of spheres. This study was limited to the first mode of resonance. Blom determined experimentally the intrinsic quality factor of silicon which is comparable with that of quartz. Zhang et al. [5] developed a closed-form solution for a rigid structure placed parallel and moving vertically to the wall. Starr [6] developed a numerical solution of an elastic structure where the gap changes in the wedge-like shape. This analysis was performed for two different elastic silicon structures where the first had a rectangular geometry and the second a cylindrical one. This study was also limited to the first vibrational mode. Cho et al. [7] analyzed the influence of lateral vibrations on both the free-space and narrow-gap damping. The relationship between the four damping factors (structural damping, viscous damping, acoustic damping and friction) has not been clarified yet. Hosaka et al. [8] provided a closed-form solution for the damping forces caused by the airflow and squeeze forces for oscillators of arbitrary shape and for an arbitrary number of vibrational modes. These results were experimentally validated and compared to the results provided by Cho et al. [7]. Hosaka and Uenishi [9] studied four damping ratios for the silicon and Permalloy materials. They experimentally and theoretically showed that viscous air damping is more significant in the second vibrational mode that in the first one. They also showed that the internal material damping remained constant and did not depend on actuator length. When a rigid body is close to the vibrating structure, damping is generated by squeeze forces which are inversely proportional to the beam length. In the absence of this rigid body or for large separations, the damping is generated by airflow forces. Hutcherson and Ye [10] studied squeeze damping on a micro-resonator and demonstrated using the Christian model and the Bao model, through simulation and the experiment, that the quality factor is very large when the air pressure approaches a secondary vacuum. It remains significant in a primary vacuum, but becomes very low at atmospheric pressure. One also can note that no acoustic radiation should occur under such conditions, significantly reducing the possible sources of damping. In the experiment conducted by Andrews et al. [11], the measured quality factor of an oscillating micro-beam decreases when the pressure increases from 1 to 10^6 Pa, indicating that viscous air damping is the dominant loss mechanism within this pressure range. Zooh et al. [12] compared measurements of the phase and amplitude response of an electro-statically driven silicon microstructure with values expected from squeeze film damping. The structure is approximated by two closely spaced parallel plates separated by a narrow air gap and oscillating perpendicular to each other. It was shown that at frequencies below 1 kHz, the difference between the force function and the plate motion could be related very simply to gas viscosity. In a recent paper, Andrews and Harris [13] measured the effective viscosity of the five following gases: Argon, O_2, N_2, CO_2, H_2 and air, at various pressures between a secondary vacuum and atmospheric pressure. The evolution of the viscosities of these different gases and air is nonlinear with respect to the pressure. In addition, when the pressure is close to a vacuum, the viscosity of the various gases as well as that of air tends towards zero.

In this paper, the effect of air on the dynamic behavior of a small cantilever beam is investigated. Initially, an experimental study using a white noise excitation is presented. The analysis of the recorded Frequency Response Functions (FRF) is performed using a linear curve fitting technique. The white noise excitation is then replaced by a free response, or drop-sine excitation, that will be called here a ''dynamic release test''. The analysis of the measurement signal is realized by a continuous wavelet transform, noted ''WT'', with complex values. Since a general description of the identification technique is reported by Kumar and Foufoula-Georgiou [14] and Mallat [15], only a brief review of this approach is reported here. The amplitude of the wavelet transform is related to the equivalent modal damping coefficient and its phase is related to the equivalent modal frequency of the considered mode, as shown by Ruzzene et al. [16]. In this context, Slavic et al. [17] identified the damping coefficient of a free–free structure, using a wavelet transform based on the Gabor function. Lardies and Gouttebroze [18] used a similar technique, based on the general modified Morlet wavelet, to identify the dynamic behavior of the Nanjing building in China. Lardies et al. [19] minimized the entropy of the wavelet transform in order to obtain a parameter depending on both frequency and time. Heller [20] characterized the nonlinear behavior of large-scale bolted structures by using the same general modified

Morlet wavelet. The dynamic release test was used to identify the nonlinear frequency and damping defined by Heller [20] as the equivalent model frequencies and the equivalent model damping. The same technique will be applied in this paper to the first bending mode of a small cantilever beams. In the last part of this paper, a description of the theoretical Hosaka model for airflow damping and squeeze damping is presented and compared to the experimental results.

2. Experimental setup

The experiment was designed to study the influence of both air and the excitation force on the dynamic behavior of a structure, which is connected to a electromagnetic shaker through an aluminum support. The beam is 0.36 mm thick, 3.6 mm wide and 15 mm long. It is attached to the support with four screws at a distance of 7.8×10^{-3} m from the free end of the beam. An accelerometer is also fixed to the aluminum support system in order to record the acceleration amplitude imposed by the electromagnetic shaker. The whole setup, including the electromagnetic shaker, the support system, the beam, and the accelerometer is placed in a lined enclosure (Fig. 1). A tight borosilicate porthole is used as a lid. It ensures the transmission of approximately 90% of a general wave whose amplitude varies between 400×10^{-9} and 700×10^{-9} m. The enclosure is connected to a vacuum pump in order to create a primary vacuum monitored by a pressure gauge. The time response velocity of the beam is recorded without contact by a Doppler vibrometer [21]. The assembly is excited by a Brüel and Kjaer (B&K) electromagnetic shaker used in the vertical position. The acquisition and signal generation are carried out by a multichannel dynamic signal analyzer (SigLab).

The characterization is performed for three different materials: silicon, lithium niobate and quartz. Because lithium niobate and quartz are transparent materials, a thin aluminum layer ($\sim 0.35 \times 10^{-6}$ m) is sputtered on the top face of the beam. The average arithmetic roughness of these materials, as measured by a micro-profilometer, is reported in Table 1.

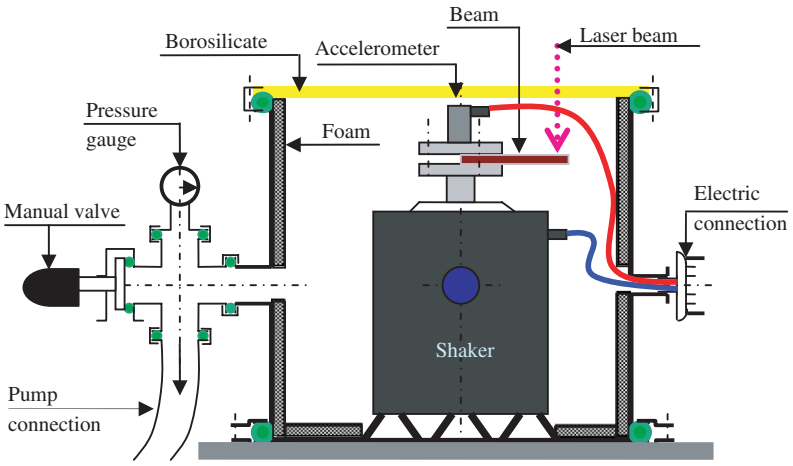

Fig. 1. Simplified diagram of the experiment.

Table 1
Depth of average of the arithmetic roughness of materials

Materials	Silicon (nm)	Lithium niobate (μm)	Quartz (μm)
Depth of average arithmetic roughness (smooth face)	<1.00	0.02	0.03
Depth of average arithmetic roughness (matt face)		0.25	0.21

3. Linear identification from white noise

3.1. Measurement procedure

A series of tests were performed with a white noise force in the frequency range of 0–10 kHz for several different levels of root mean square (rms) base acceleration. For each test, the FRF between the response of the beam measured by the Laser Doppler vibrometer (velocity response of the free end of the beam) and the white noise excitation measured by the accelerometer (acceleration signal of the assembly) was recorded via the SigLab multichannel analyzer. An example of the white noise excitation and the corresponding response is presented respectively in Fig. 2a and b for the quartz structure. Fig. 3 shows four FRFs corresponding to four different excitation levels on the same quartz structure. The nonlinear behavior of the structure is visible since the amplitude and frequency of the resonance peak vary. On the other hand, the peaks remain quasi-symmetric indicating that the nonlinearities are small. An examination of the coherence functions revealed that they were very weakly affected by the nonlinear behavior, especially after averaging.

Before each series of measurements, a relevance check was also carried out by focusing the laser beam on the accelerometer placed on the support system excited by the electromagnetic shaker. Then, the FRF between

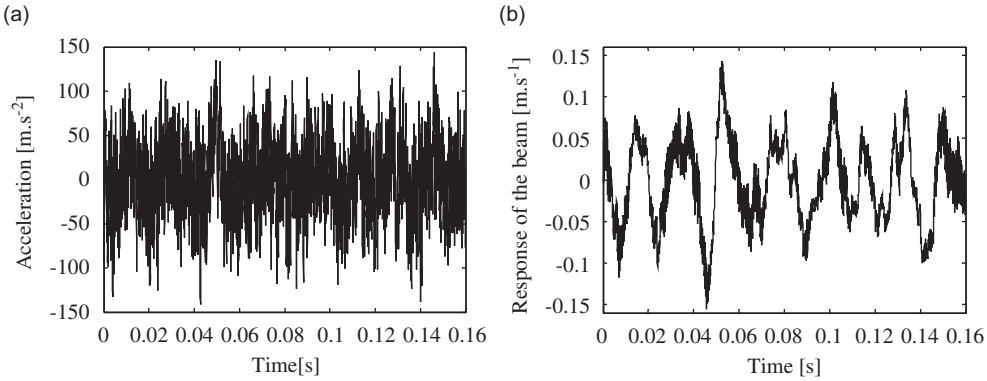

Fig. 2. (a) Example of the white noise excitation of the assembly (quartz structure); (b) response of the free end of the quartz structure.

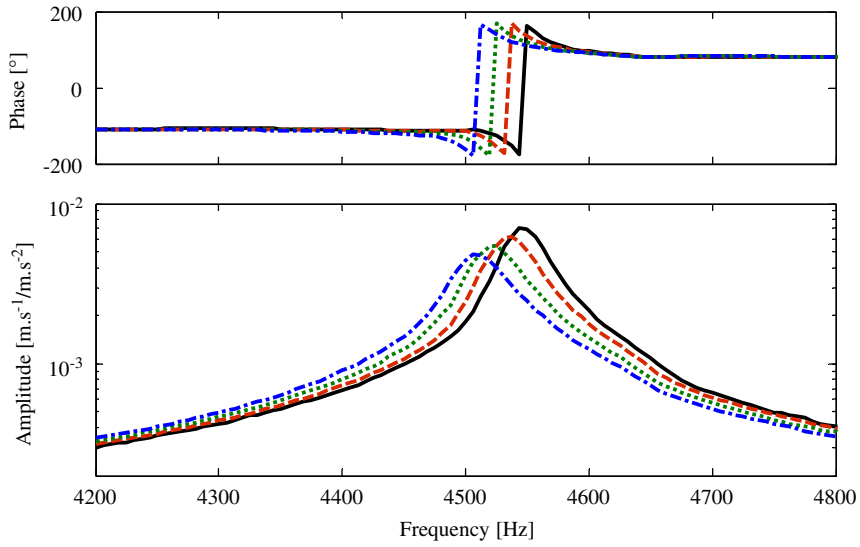

Fig. 3. Example of FRF amplitude and corresponding phase obtained on quartz structure. ——— rms = 0.009 m s^{-2}; - - - - rms = 0.025 m s^{-2}; . . . . . rms = 0.06 m s^{-2}; – · – · – rms = 0.2 m s^{-2}.

the time derivative of the velocity response and the accelerometer signal was checked to be constant and unitary over the frequency range. The laser was then focused on the free end of the beam. Finally, the modal frequency and the damping ratio associated with the first bending mode of the beam were identified by a linear curve fitting technique for various levels of air pressure ranging from a primary vacuum to atmospheric pressure and for various base accelerations of white noise levels.

3.2. Experimental uncertainties

In order to quantify experimental uncertainties, two kinds of repetitivity tests were carried out on the quartz structure. For the first test, two series of measurements at different base acceleration levels were successively performed with the second series initiated immediately after the first one. The identified modal frequencies for the first and the second measurement series are plotted in Fig. 4a. The maximum frequency variation, between the first and the second measurements is equal to 5 Hz, which corresponds to a relative frequency variation of 0.2%. This small uncertainty is mainly caused by the measurement process and shows that the experimental setup and procedure are reliable.

The second test was similar to the first one, except that the second set of measurements was performed 48 h after the first set. Fig. 4b illustrates a maximum frequency variation equal to 80 Hz corresponding to a maximal relative frequency variation of 1.7%. We assume that this dispersion is related to the intrinsic structural variation of the materials due to time relaxation. This result shows that the measurements have to be performed in a period as short as possible in order to be comparable.

3.3. Results

Fig. 5a shows that the modal frequency is only slightly influenced by the excitation level and the pressure variation with the frequency variation relative to the pressure change not exceeding 10 Hz. In Fig. 5b, it is clear that the damping ratio varies with the excitation level, indicating a nonlinear behavior of the beam. The pressure variation also affects the results. The damping variation between the primary vacuum and the atmospheric pressure is almost constant (approximately 0.017%) [22].

The experiments are also carried out on quartz and lithium niobate structures. In the case of quartz, the base acceleration and pressure both have a slight influence on the modal frequency (Fig. 6a). The base acceleration variation causes a maximum frequency shift equal to 65 Hz and the pressure variation causes a maximum frequency shift equal to 30 Hz. The damping ratio was also affected by the base excitation and the pressure and it increases up to a maximum value equal to 0.61% at atmospheric pressure and 0.53% at a primary vacuum for a base acceleration equal to $0.6\,m\,s^{-2}$ (Fig. 6c).

After this maximum, the damping ratio slowly decreases until the rms base acceleration reaches $1.1\,m\,s^{-2}$. We then remark a tendency to increase. In the case of lithium niobate, the rms base acceleration also clearly

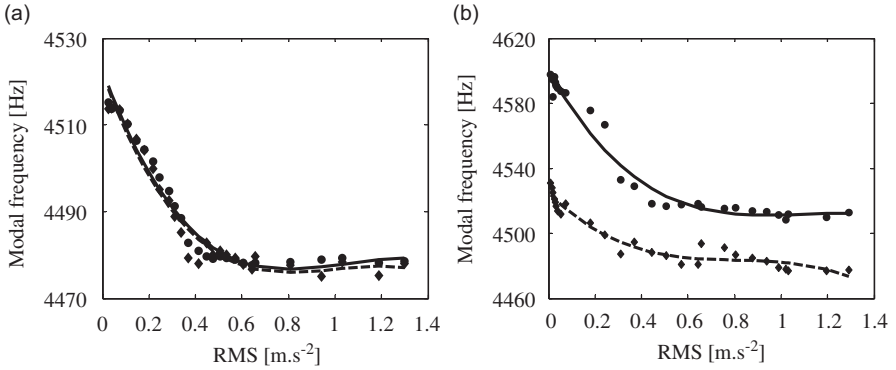

Fig. 4. Modal frequency evolution versus base acceleration (rms): quartz beam; (a) successively series of measurements; (b) 48 h delay between the two series of measurements. *Symbols*: experimental values; lines: polynomial fitting. ◆ and - - - - first measurement; ● and ——— second measurement.

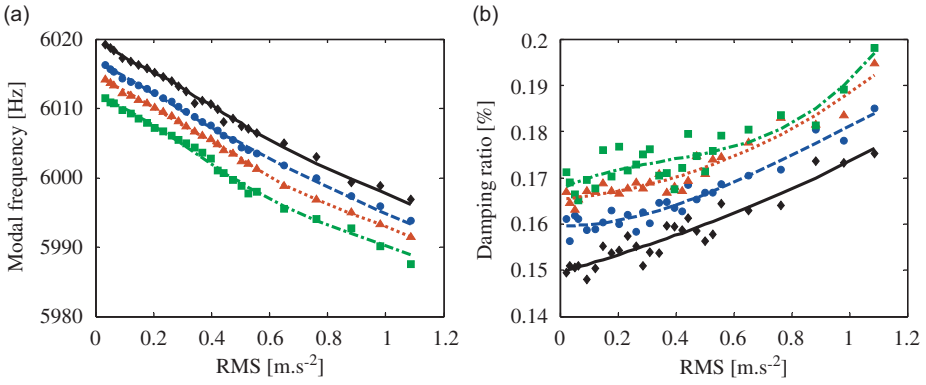

Fig. 5. Silicon beam. (a) Identified modal frequency: silicon structure; (b) identified modal damping; symbols: experimental values; lines: polynomial fitting. ◆ and ——— primary vacuum; ● and - - - - pressure ~300 mbar; ▲ and . . . . . pressure ~600 mbar; ■ and – · – · – atmospheric pressure.

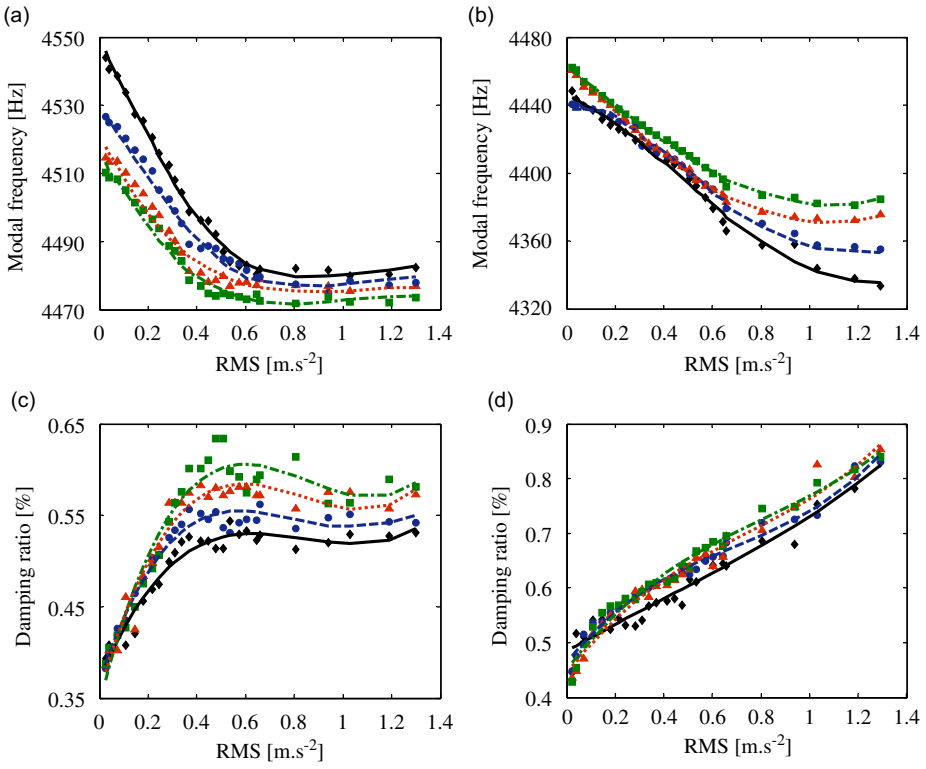

Fig. 6. (a) Identified modal frequency: quartz structure; (b) identified modal frequency: lithium niobate structure; (c) identified modal damping: quartz structure; (d) identified modal damping: lithium niobate structure; symbols: experimental values; lines: polynomial fitting. ◆ and ——— primary vacuum; ● and - - - - pressure ~300 mbar; ▲ and . . . . . pressure ~600 mbar; ■ and – · – · – atmospheric pressure.

affects the modal frequency (maximum shift equal to 100 Hz) and the damping ratio (maximum variation equal to 0.4%), but the effect of air viscosity was not clearly visible (Fig. 6b and d).

In conclusion, while the tests with a white noise made it possible to study the effect of airflow on the dynamic behavior, they also revealed a significant nonlinear dynamic behavior. Furthermore, this measurement and identification technique required a significant amount of computation time. As a

consequence, a new nonlinear identification technique based on the free response of the tested structure was employed in order to determine the modal parameters.

4. Nonlinear identification from the free responses

The dynamic behavior of a slightly nonlinear system results in a strong dependence of the frequencies and damping on the amplitude of vibration of the structure. On the other hand, the dynamic behavior for a constant response amplitude is often assumed to be linear. Sine stepping measurements can thus be carried out with a constant amplitude response for a set of selected amplitudes. For each measurement, a linear identification technique provides the characteristics of the model associated with the given amplitude of vibration. In this way, a discrete description of the nonlinear dynamic behavior is obtained. The major disadvantage of this method is the long measurement time necessary for a relatively small quantity of information.

Recently, a time–frequency approach for free responses was developed [18,19]. It has the advantage of providing a quasi-continuous description of the parameters (instantaneous frequency and damping as well as equivalent modal frequency and damping) from only one time response. The principle is simple and is based on treating the free response of the structure like the response of a nonlinear oscillator with only one degree of freedom. This response makes it possible to sweep a whole range of amplitudes in only one measurement. The continuous WT of the recorded signal is then calculated and used to identify the instantaneous frequency and damping.

4.1. Continuous wavelet transform (WT)

The continuous WT can be explained by analogy with the Fourier transform. In both cases, the considered signal is represented by a linear combination of basic functions. For the Fourier transform, the basic functions are trigonometric functions covering the entire considered time interval, more or less dilated by a frequency parameter. For the continuous WT, the basic functions are deduced from a reference function, called the mother wavelet, defined in time and allowing the description of the signals for a localized frequency. A very common mother wavelet is the general modified Morlet wavelet

$$\Psi(t) = \mathrm{e}^{(\mathrm{j}\omega_0 t)}\,\mathrm{e}^{-t^2/N}, \tag{1}$$

where ω_0 is the wavelet frequency and N is the parameter which controls the shape of the basic wavelet ($N>0$). The dilated Fourier transform version of the modified Morlet wavelet is presented as

$$\hat{\Psi}(\omega) = \mathrm{e}^{(N/4)(\omega-\omega_0)^2}. \tag{2}$$

An important value of N gives a narrower spectrum allowing a better frequency resolution. The optimal value of N is obtained by minimizing the entropy of the wavelet coefficient (see Ref. [23] for more details). The continuous WT gives time and frequency information about the analyzed data. The basis functions are deduced from the Morlet mother wavelet which is dilated by a scale parameter u defining the size of analyzing window and localized in the time domain by a position parameter v:

$$\Psi_{(v,u)}(t) = \frac{1}{\sqrt{u}}\,\Psi\left(\frac{t-v}{u}\right). \tag{3}$$

The continuous WT of a temporal signal $x(t)$ at the scale u and at the position v is calculated by correlating with the corresponding wavelet [15]:

$$T_x^{\Psi}(u,v) = \frac{1}{\sqrt{u}}\int_{-\infty}^{+\infty} x(t)\overline{\Psi\left(\frac{t-v}{u}\right)}\,\mathrm{d}t, \tag{4}$$

where $\bar{\Psi}$ is the complex conjugate of $\Psi(t)$. The skeleton of the continuous WT is the modulus of the continuous WT coefficient $|T_x(u,v)|$ that represents a surface in the time–frequency space (Fig. 7a). The ridge of the continuous WT is the locus $(u_r(v), v)$ of local maxima on the continuous WT skeleton, which is described

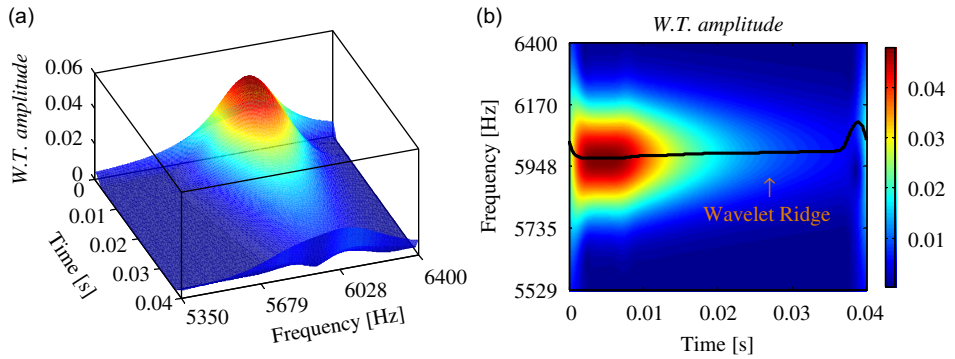

Fig. 7. Silicon beam: (a) amplitude of the continuous WT for the free response; (b) ridge of the continuous WT amplitude for the free response.

by Eq. (5) and represented in Fig. 7b. For more details, see Ref. [23]:

$$\left|T_x(u_r(v),v)\right| = \max_u\left(\left|T_x(u,v)\right|\right). \tag{5}$$

4.2. Identification of equivalent modal parameters

By using the theory of asymptotic signals [24], a slightly nonlinear oscillator can be characterized by its equivalent modal frequency $\omega_e(a)$ and damping $\zeta_e(a)$, where the parameter a denotes the amplitude of vibration. These two parameters can be identified thanks to the continuous WT. A brief discussion of the major issues of the procedure is given in Heller [20]. The first step consists in computing the continuous WT of the resonator free response and locating its ridge. It has been shown that the resonator instantaneous frequency is equal to the time derivative of the argument of the continuous WT ridge:

$$\omega_e(v) = \frac{\mathrm{d}}{\mathrm{d}v} Arg[T_x(u_r(v),v)]. \tag{6}$$

The instantaneous damping coefficient is obtained from the logarithmic decrement of the modulus of the continuous WT ridge:

$$\zeta_e(v) = -\frac{1}{\omega_0}\frac{\mathrm{d}\,\ln\left(\left|T_x(u_r(v),v)\right|\right)}{\mathrm{d}v}, \tag{7}$$

where ω_0 is the natural angular frequency of the undamped system. The second step consists in identifying the envelope of the signal. In our case, the measurements were achieved using a laser vibrometer. It was thus necessary to integrate the signal in order to obtain a displacement envelope. Finally, the equivalent modal frequency and damping are obtained by combining the instantaneous parameters and the envelopes. Note that the natural angular frequency ω_0 is equal to ω_e ($a = 0$), and is obtained by an extrapolation of $\omega_e(a)$ for a small amplitude range. It also must be stated that the beginning and the end of the modulus of the continuous WT cannot be used because of edge effect [17]. Note that the edge effect can be reduced by adding zeros or by adding negative values of the signal at the beginning and the end of the signal.

4.3. Dynamic release tests results

The assembly described previously was excited by a stepped sine force on one of its resonance frequencies. The free response of the structure was then recorded using the laser vibrometer (Fig. 8).

Many tests were carried out with various pressures ranging from a primary vacuum to atmospheric pressure and with various excitation amplitudes at the beginning of the test (0.1, 0.15 and 0.2 $\mathrm{m\,s^{-1}}$). Only the results associated with the first mode are presented here, respectively for silicon, quartz and lithium niobate.

Fig. 9 shows an example of the envelopes obtained at different air pressures for the silicon beam. The effect of airflow damping is clearly visible. The instantaneous parameters (Fig. 10a and 10b) and equivalents modal

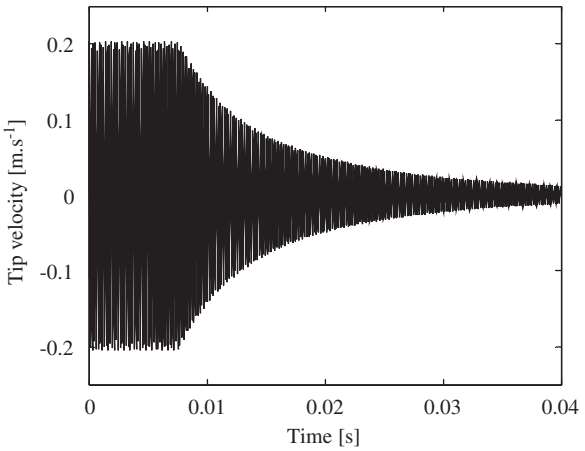

Fig. 8. Signal measured by the laser vibrometer at the beam free end.

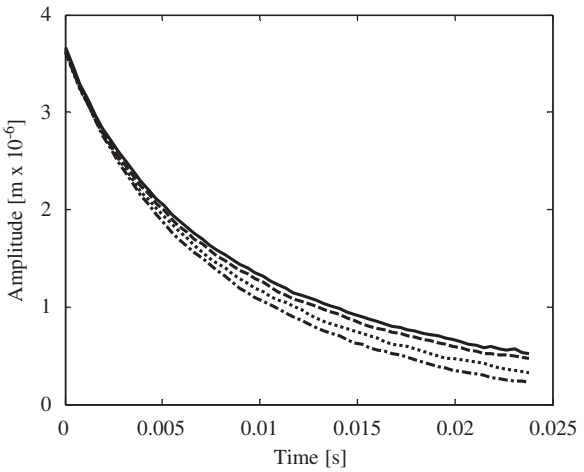

Fig. 9. Silicon beam: envelope of the measured mode in time domain. ——— primary vacuum; - - - - pressure ~300 mbar; . . . . . pressure ~600 mbar; – · – · – atmospheric pressure.

parameters (Fig. 10c and 10d) are presented for an initial excitation amplitude equal to $0.2\,\mathrm{m\,s^{-1}}$. The variation of pressure from a primary vacuum to atmospheric pressure produces a frequency shift equal to 8 Hz and remains constant with respect to time and vibration amplitude. The equivalent damping identified using these measurements is significant and corresponds to a nonlinear behavior. When the pressure varies from a primary vacuum to atmospheric pressure, the variation of the equivalent damping is equal to 0.017%. This value of damping variation agrees with the analytical airflow damping and experimental airflow damping obtained by a white noise excitation.

Both instantaneous parameters (Fig. 11a and 11b) and equivalents parameters (Fig. 11c and 11d) are presented for three levels of initial excitation amplitude, respectively, equal to 0.1, 0.15 and $0.2\,\mathrm{m\,s^{-1}}$ and at a primary vacuum. A drop in the initial excitation amplitude produces a reduction of all of the instantaneous damping and the equivalent modal damping values. From a value of the time equal to 0.0175 s and from a value of the vibration amplitude for the free end of the beam equal to $1.4\times10^{-6}\,\mathrm{m}$ downward, the instantaneous damping and equivalent modal damping are the same. This remark indicates that the results corresponding to the zone where the curves are not superimposed are due to the transient effects following the forced excitation. Nevertheless, the fact that the other parts of the curves are superimposed validates the

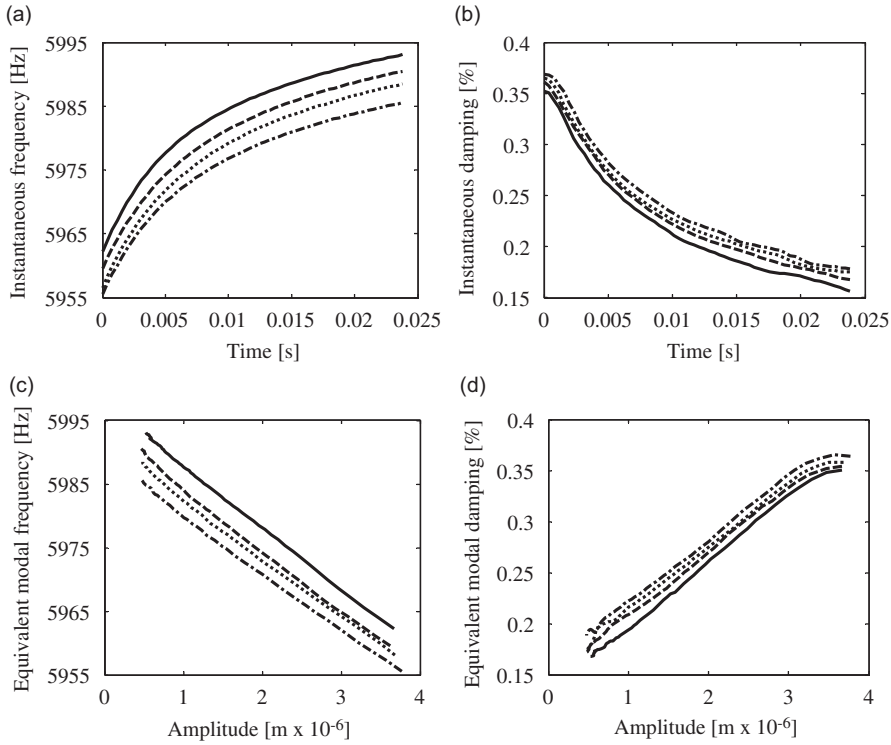

Fig. 10. Silicon beam: (a) instantaneous frequency; (b) instantaneous damping; (c) equivalent modal frequency; (d) equivalent modal damping. ——— primary vacuum; - - - - pressure ~300 mbar; . . . . . pressure ~600 mbar; – · – · – atmospheric pressure.

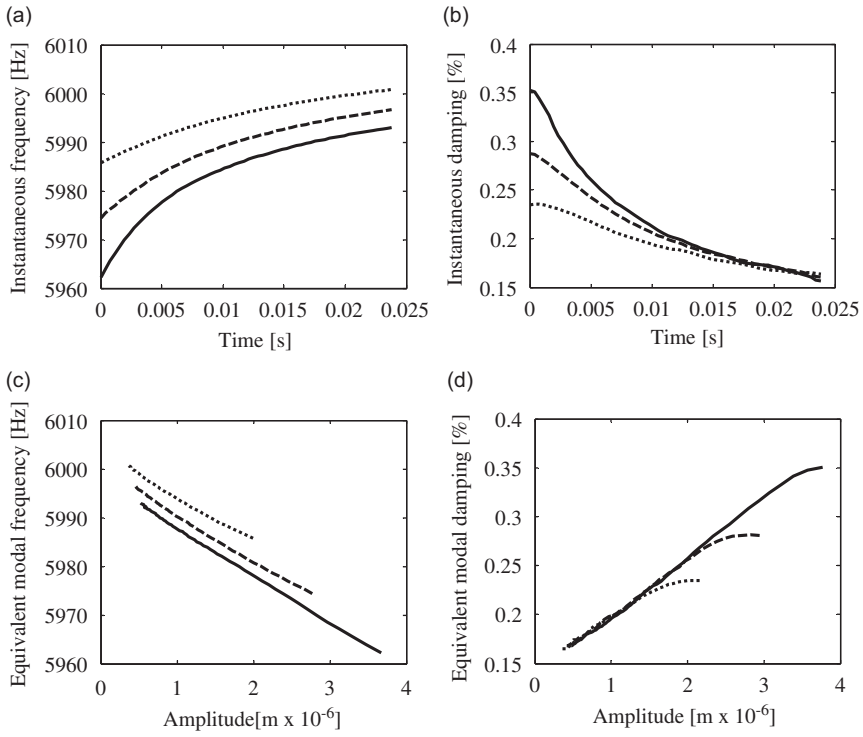

Fig. 11. (a) Instantaneous frequency; (b) instantaneous damping; (c) equivalent modal frequency; (d) equivalent modal damping. ——— $0.2\,m\,s^{-1}$; - - - - $0.15\,m\,s^{-1}$; . . . . . $0.10\,m\,s^{-1}$.

principle that a single measurement with a high initial excitation allows the modal identification to be performed over the whole range of amplitudes.

In Fig. 12, only the equivalent modal frequency and damping identified on the quartz structure are presented for initial excitation amplitude equal to $0.2\,\mathrm{m\,s^{-1}}$. The equivalent damping is much higher than for the silicon structure and exhibits a strongly nonlinear behavior. The evolution of the equivalent modal damping shows a first localized maximum corresponding to small vibration amplitudes. This result agrees with the experimental results carried out with the white noise excitation. A second maximum is clearly visible and equal to 1.7% at atmospheric pressure and 1.4% at primary vacuum. The equivalent modal damping variation, with respect to the pressure variation, is maximal when the vibration amplitude corresponds to the second maximum damping identified at atmospheric pressure and is equal to 0.5%. The equivalent modal frequency shift due to the pressure variation is seen to be nonlinear.

The equivalent modal frequency evolution, identified from the dynamics of the lithium niobate beam under different levels of air pressure, also shows a nonlinear behavior as for the quartz structure. The pressure variation between a primary vacuum and atmospheric pressure produces a small frequency variation at low vibration amplitudes. This frequency variation is equal to 50 Hz when the vibration amplitude exceeds $10^{-6}\,\mathrm{m}$ (Fig. 13a).

The identified equivalent modal damping of the lithium niobate structure exhibits a strongly nonlinear behavior with the presence of a maximum. It is of the same order of magnitude as for the quartz structure and can reach 1.7% at atmospheric pressure and 1.5% at a primary vacuum for a vibration amplitude equal to $1.2\times10^{-6}\,\mathrm{m}$ (Fig. 13b). Before the maxima, the influence of air viscosity remains difficult to identify, which is

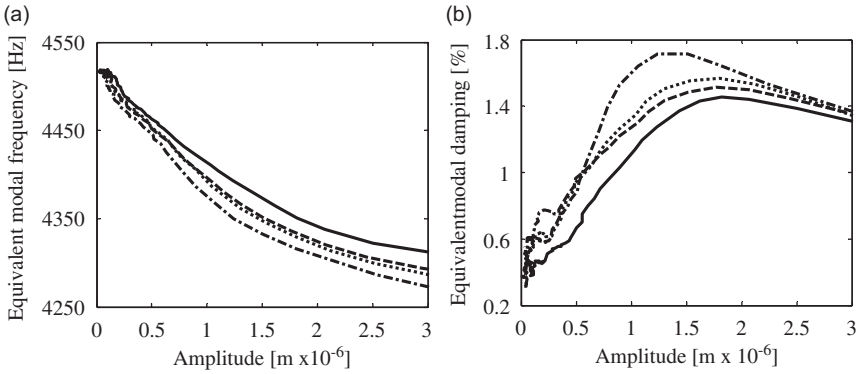

Fig. 12. Quartz beam: (a) equivalent modal frequency; (b) equivalent modal damping. ——— primary vacuum; - - - - pressure ~300 mbar; . . . . . pressure ~600 mbar; – · – · – atmospheric pressure.

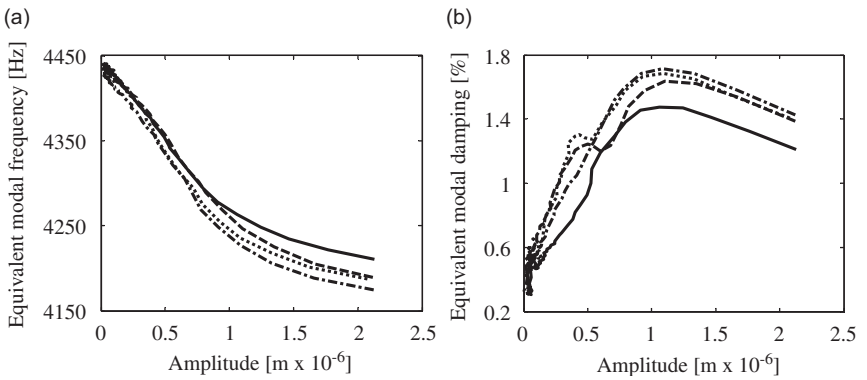

Fig. 13. Lithium niobate beam: (a) equivalent modal frequency; (b) equivalent modal damping. ——— primary vacuum; - - - - pressure ~300 mbar; . . . . . pressure ~600 mbar; – · – · – atmospheric pressure.

in agreement with the experimental results carried out with the white noise excitation. When the equivalent damping passes over the maxima, the influence of the air viscosity becomes clearly visible and constant. The equivalent damping variation due to the pressure variation from a primary vacuum and atmospheric pressure is equal to 0.2% in this zone.

Finally, for the three studied structures, the effect of the airflow damping is clearly present but it remains relatively weak compared to the stick-slip damping resulting from friction between the contact interfaces at the clamped end of the structure.

5. Energy losses in a mechanical structure

5.1. Origin of energy losses

The dynamic response amplitudes of vibrating structures are limited by the dissipated energy. The dissipation sources of energy can vary: stick-slip ξ_1, intrinsic material dissipation ξ_2, thermoelastic dissipation ξ_5, acoustic radiation in the interfaces and in the surrounding media ξ_6, and finally viscous dissipation due to the presence of trapped air (squeeze effect) ξ_3 and free air ξ_4 (airflow) (Fig. 14). These various dissipation sources have several degrees of influence on the structural dynamics that is related to the quality factor (Q-factor). The Q-factor is defined as the relation between the dissipated energy and the total energy of a vibrating structure per period:

$$Q\text{-factor} = \frac{2\pi \times (\text{Total energy in the system})}{\text{Dissipated energy}} = \frac{2\pi U_i}{U_d}. \tag{8}$$

When the dissipation is high, the quality factor Q is small and vice-versa. The relationship between the total damping and the quality factor is defined by

$$\xi = \xi_1 + \xi_2 + \xi_3 + \xi_4 + \xi_5 + \xi_6 = \frac{1}{2Q}. \tag{9}$$

5.2. Internal material damping

The internal attenuations are explained as the phenomena appearing in a material under the effect of an irreversible strain or stress (molecular diffusion, mutual movement between grains: inter-granular slip, twins, dislocation translation, etc.). Intrinsic damping depends strongly on the stress amplitudes, on the temperature reached during a surface treatment, on the mechanical behavior of the material (elastic behavior, plastic behavior or combined behavior with viscosity effect) and on the boundary conditions. For most single-crystal materials, poly-crystal materials and metals, internal damping is relatively weak. In the case of silicon, the experimentally identified structural coefficient is equal to 5×10^{-6}. The value of internal damping is equal to

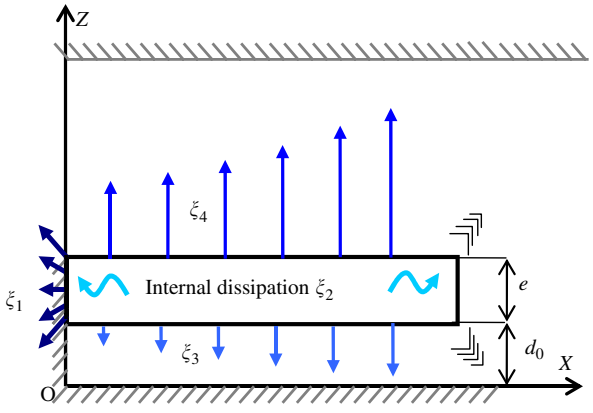

Fig. 14. Explanatory diagram of various damping.

half of this structural coefficient ($2.5 \times 10^{-4}\%$). The internal damping is higher for composites, plastic materials and wood.

5.3. Thermoelastic damping

Thermoelastic phenomena are classified among the most significant mechanisms of energy loss in oscillators. It results from a coupling between the mechanical behavior of the material and thermodynamics [25–27]. In these oscillators, vibrations induce non-uniform levels of stresses and consequently temperatures variations are created in the same material. A thermodynamic energy flux appears between areas at different temperatures and results in energy losses. This damping can reach significant values in the case of a vibrating structure (around $10^{-2}\%$) [28].

5.4. Acoustic radiation

If the vibrating device is placed in an open fluid (or large enough with respect to the device dimensions), a fluid–structure coupling occurs that generates acoustic radiation in the fluid medium. Considering for example a cantilever beam vibrating in open air, a part of the elastic energy trapped in the environment is converted to acoustic radiation at each vibration cycle, reducing the quality factor of the whole system. This can be accounted for by an appropriate simulation of the influence of the fluid medium on the vibrating structure, for instance combining a Green's function representation of the effect of the open medium to localize vibration via boundary element methods [29].

5.5. Stick-slip at the clamped end of the cantilever beam

Vibration of a structure assembled with screws produces significant microsliding between the beam and materials in contact with it. The beam and the material surfaces are never perfectly smooth and have irregularities even if they are carefully polished and the application of a tightening torque creates a normal load [30]. The contact is established by the means of the asperities in discrete zones. On the scale of the microgeometry contact, the microsliding phenomenon results in three principal states:

- Elastic strain, then plastic stain with interpenetration of asperities.
- Development of an adhesive connection.
- Shearing of joining followed by an elastic relaxation of the asperities.

The origins of resistance to microsliding are the interactions between the asperities where the local energy dissipation phenomenon occur during the different stages of the formation and the separation of the microcontact, thus reducing the quality factor of the whole system [31]. This phenomenon depends strongly on the material contact rigidity [32,33].

5.6. Viscous air damping

The vibration of a clamped beam in contact with air generates viscous damping. The origins of this energy dissipation can be separated into two phenomena. The first is caused by the squeeze effect due to the presence of a rigid body near to the vibrating beam and the second is due to the contact of the beam with airflow.

5.6.1. Squeeze damping

When a vibrating structure is placed close to a rigid wall, a squeeze force appears due to the gap between them. This force is calculated from the Reynolds equation:

$$\frac{\partial}{\partial x}\left(d^3\frac{\partial P}{\partial x}\right)+\frac{\partial}{\partial y}\left(d^3\frac{\partial P}{\partial y}\right)=12\mu\left(\frac{\partial d}{\partial t}\right), \tag{10}$$

where P is the air pressure, μ the air viscosity (a parameter which depends on the pressure), d the gap and y the axis along the beam width. In order to seek a solution for Eq. (10), the following assumptions are taken into account: the length of the beam L is much greater than its width l, the pressure gradient in the longitudinal direction is negligible, the initial gap d_0 is uniform, the vibration amplitude of the beam λ is much smaller than the initial gap and the boundary condition P_0 is null along the width of the beam equal to $(\pm y/2)$. The actual gap is represented by $d = d_0 + \lambda$. The expression of the squeeze force per unit length is obtained by integrating the simplified Reynolds equation over the beam width $(\pm y/2)$:

$$d_0^3\left(\frac{\partial^2 P}{\partial y^2}\right) = 12\mu\left(\frac{\partial \lambda}{\partial t}\right) \Rightarrow F = \frac{\mu l^3}{d_0^3}\left(\frac{\partial \lambda}{\partial t}\right). \tag{11}$$

The squeeze force damping is represented by the Hosaka equation:

$$\xi_3 = \frac{\mu(p) l^2}{4\pi e \rho_b d_0^3 f_n}, \tag{12}$$

where ρ_b is the beam density, f_n the natural frequency and e the thickness of the beam. According to this last equation, damping depends on material, geometry, excitation and gap size. In our calculations, the beam dimension was those used in the experiments (working length $L = 7.8 \times 10^{-3}$ m, width $b = 3.6 \times 10^{-3}$ m, thickness $e = 0.36 \times 10^{-3}$ m). The frequencies are calculated from the Bernoulli equation (Eq. (13)) for thickness values in the range $[0.2, 0.6]$ mm:

$$f_i = \frac{\alpha_i^2}{2\pi L^2}\sqrt{\frac{EI}{\rho_b S}}, \tag{13}$$

where E is the Young modulus, I the quadratic moment of inertia, S the section, L the free length, ρ_b the density of silicon and α_i a parameter which depends on the vibrational mode ($\alpha_i = 1.8751$ for the first mode). The gap value used for our calculations is equal to the distance that separates the beam and the shaker (4×10^{-3} m) and it is the smallest distance which separates the beam and its surrounding surfaces. The evolution of squeeze damping versus the beam thickness is nonlinear (Fig. 15), knowing that this damping is calculated just for a quarter of a vibrational period. Under these boundary conditions, the damping is very small which means that the effect of the squeeze force is negligible. However, when the gap decreases, the damping increases considerably. For example, damping increases from 10^{-6} to 10^{-3}% when the gap decreases from 4×10^{-3} to 0.6×10^{-3} m. These values of squeeze damping confirm that it is strongly related to the gap value.

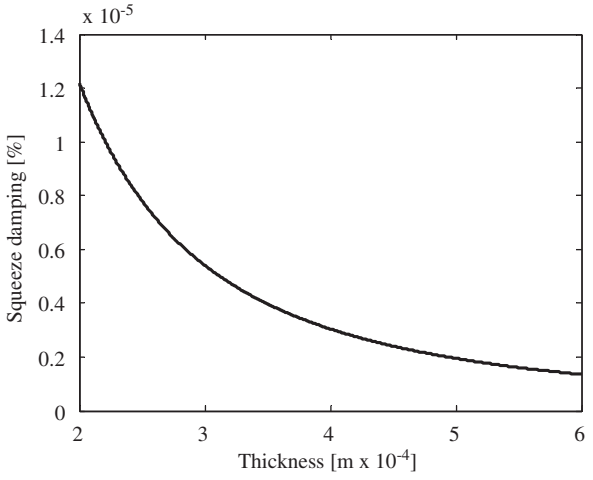

Fig. 15. Squeeze damping evolution versus thickness.

5.6.2. Airflow damping

The airflow around the dynamic oscillator along the axis (Oz) is described by the Navier–Stokes equation:

$$\overrightarrow{\text{grad}}P = \mu\Delta\vec{v} + \rho_a\vec{F} - \rho_a\frac{\mathrm{d}\vec{v}}{\mathrm{d}t}, \tag{14}$$

where i and j vary from 1 to 3 and ρ_a, $\vec{v}$ and $\rho_a\vec{F}$, are, respectively, the air density, the velocity and the volume force. Because the Navier–Stokes equation cannot be solved analytically, some approximations were considered. The maximum vibration velocity ($v = a\omega$, with a the oscillation amplitude of the beam end and ω the angular frequency) is calculated to estimate both the Reynolds and Valensi numbers which are respectively the ratios of the second and the third term with respect to the first term on the right-hand side of the Navier–Stokes equation. During our calculations, the natural frequency of the first bending mode varies between 5995 and 6010 Hz corresponding to maximum velocity values ranging from 2×10^{-3} to $1.1\times10^{-2}\,\mathrm{m\,s^{-1}}$. The Reynolds numbers are estimated by the following approximation (Eq. (15)) and are smaller than 1 which means that the second term is negligible compared to the first:

$$R_e \approx \frac{\rho_a e v}{\mu} \Rightarrow \left\{5.2\times10^{-2} \leqslant R_e\left(m^{-1}\right) \leqslant 3\times10^{-1}\right. . \tag{15}$$

The Valensi numbers are estimated by the following approximation:

$$R_v \approx \frac{2\pi\rho_a e^2 f_n}{\mu} \Rightarrow \left\{350 \leqslant R_v\left(m^{-1}\right) \leqslant 352,\right. \tag{16}$$

and is calculated for the same frequency and velocity values. The Valensi numbers are much larger than the Reynolds numbers by a factor of 10^4. For a small silicon structure of a few millimeters, we cannot neglect the third term of Eq. (14) because Valensi number is too large. Eliminating the second term from the Navier–Stokes equation gives the basic airflow equation. This new expression cannot be solved analytically in the closed-form for our beam-shaped oscillator but a numerical analysis is possible. Consequently, Hosaka attempted to obtain an approximate solution by using a known solution for another vibrating body. When the beam length is much larger than the other dimensions, the airflow equation is assumed to be bidimensional. The stream line is thus determined only by the beam velocity and width, when the thickness is smaller than the width. In the case of a sphere, the airflow equation is 3D. Its spatial derivative is the same as a beam when the sphere diameter is equal to the beam width. When the sphere moves synchronously with the beam, the time derivative is also the same for the sphere and the beam. Therefore, all the terms on the right-hand side of Navier–Stokes equation have the same order of magnitude for airflows around the sphere and the beam, from which we conclude that the airflow pressure on the left-hand side has about the same order of magnitude for the beam as for the sphere. The beam then is assumed as a string of identical spheres. The airflow damping is

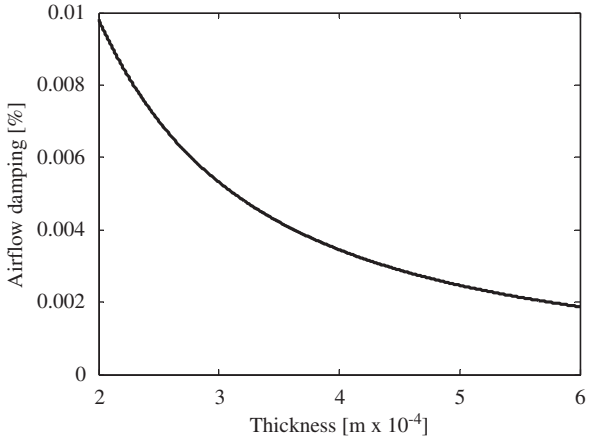

Fig. 16. Airflow damping evolution versus thickness.

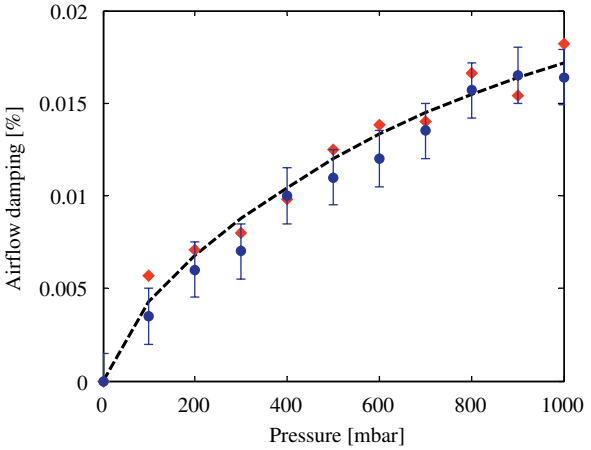

Fig. 17. Airflow damping versus pressure. – – – – theoretical airflow damping; ◆ experimental values (white noise excitation); ● experimental values (release test).

finally described by the Hosaka equation:

$$\xi_4 = \frac{3\pi\mu(p)l + 0.75\pi l^2\sqrt{4\pi\rho_a\mu(p)f_n}}{4e\pi l^2\rho_b f_n}. \tag{17}$$

As in the squeeze damping case, the airflow damping depends on material, geometry, air viscosity and vibrational mode. The computed airflow damping corresponds to the first bending mode of a silicon beam for a quarter vibration period. Fig. 16 shows its evolution versus the beam thickness. When the thickness increases, the eigenfrequency of the beam increases and the airflow damping decreases because the structure becomes more rigid. The comparison between airflow damping and squeeze damping, for a gap value equal to 4×10^{-3} m, shows that airflow damping remains largely dominant (4.5×10^{-3}%) compared to the squeeze damping (5×10^{-6}%) for a quarter of vibration period.

6. Comparison of Hosaka model and experimental results

Due to the fact that squeeze damping is negligible in our experiments, the comparison is only made between the analytical Hosaka airflow damping model and the silicon beam experiment (white noise excitation and release test). The analytical airflow damping is computed for a complete period of vibration. The experimental airflow damping is negligible in a primary vacuum and the friction damping becomes the most important effect. Therefore, the variation between the damping ratio identified at primary vacuum and the damping ratio identified at different levels of pressure and different rms levels, gives the experimental airflow damping values. This variation is obtained for ten levels of air pressure inside the enclosure. The same formula is also used for the equivalent damping identified from free response tests at ten levels of pressure and for different vibration amplitudes. A good agreement is found between the theoretical Hosaka model, the experiment based on white noise excitation and the dynamic release test (Fig. 17). Though, both model and experiment show a nonlinear evolution of airflow damping between a value close to zero and 0.017%.

7. Conclusion

The influence of energy dissipation due to the presence of the air on the dynamic behavior of small cantilever beams has been experimentally investigated. Experiments have been performed in order to quantify this dissipation for small cantilever beams made of three different materials and at different levels of the air pressure. Initially, a silicon beam has been excited by white noise and a linear modal identification technique was applied. The results show a nonlinear dynamic behavior, as well as the effect of the air viscosity. Dynamic

release tests were then performed and the identification of the equivalent modal parameters was carried out by a continuous WT technique adapted to slightly nonlinear systems. These tests have proven to be very effective since a large range of vibration amplitudes is covered by a single measurement. They also provide a much more detailed description of the equivalent modal frequencies and damping. The experimental airflow damping determined by the two series of measurements (white noise and release dynamic tests) is in good agreement with the theoretical damping given by the analytical Hosaka model.

The experimental characterization of the air effect was also carried out using white noise excitation and dynamic release tests on beams made of two materials: quartz and lithium niobate. The effect of the air viscosity is more significant, probably because these two materials are less rigid than silicon. As a consequence, when the Young modulus increases, the strain energy of the beam decreases and the equivalent modal damping drops off. The nonlinearity of the damping is also strongly related to the rigidity of the materials. Moreover, this study shows that the air effect is of secondary importance compared to the microsliding effect, which occurs between contact surfaces at the clamped end.

Finally, these results show that the energy losses due to microsliding and airflow are relatively high and they risk to dramatically reduce the efficiency of an energy microconverter. It would thus be judicious to test another assembly method, such as anodic bonding, in order to maximize the vibratory energy which will be converted into electrical energy.

Acknowledgement

This work is financed by the European Commission through the project STREP VIBES (IST-1-507911) (Vibration Energy Scavenging) in the Framework 6 program and by the Joint Energy Action of the CNRS & Minister of Research. We would like to thank Mr. Scott Cogan for language corrections.

References

[1] E.A. Avallone, *Standard Handbook for Mechanical Engineers*, McGraw-Hill, New York, 1987.
[2] Y. Jimbo, K. Ito, Energy loss of a cantilever vibrator, *Journal of the Horological Institute of Japan* 47 (1968) 1–15.
[3] T. Teresawa, Y. Kawamura, K. Sato, S. Tanaka, Pressure dependent dynamic characteristics of miniature silicon oscillator, *Bulletin of the Japan Society for Precision Engineering* 22 (1988) 49–54.
[4] F.R. Blom, S. Bouwstra, M. Elwenspoek, J.H.J. Fluitman, Dependence of the quality factor of micromachined silicon beam resonators on pressure and geometry, *Journal of Vacuum Science and Technology B* 10 (1992) 19–26.
[5] L. Zang, D. Cho, H. Shiraishi, W. Timmer, Squeeze film damping in microelectromechanical systems, *Proceeding of the ASME Winter Annual Meeting, Dynamic Systems, Measurement and Control* 40 (1992) 149–160.
[6] J.B. Starr, Squeeze-film damping in solid-state accelerometers, *IEEE Solid-State Sensors an Actuators Workshop*, Hilton Head Island, SC, USA, 1990, pp. 44–47.
[7] Y. Cho, A.P. Pisano, R.T. Howe, Viscous damping model for laterally oscillating microstructures, *Journal of Microelectromechanical Systems* 3 (1994) 81–87.
[8] H. Hosaka, K. Itao, S. Kuroda, Damping characteristics of beam-shaped micro-oscillators, *Sensors and Actuators A* 49 (1995) 87–95.
[9] H. Hosaka, Y. Uenishi, Static rigidity and natural frequency of flat permalloy springs used in electromagnetic microactuators, *The Japan Society for precision Engineering* 27 (1993) 253–258.
[10] S. Hutcherson, W. Ye, On the squeeze-film damping of micro-resonators in the free-molecule regime, *Journal of Micromechanics and Microengineering* 14 (2004) 1726–1733.
[11] M.K. Andrews, P.D. Harris, G.C. Tuner, A comparison of squeeze film theory with measurements of a microstructure, *Sensors and Actuators A* 36 (1993) 79–87.
[12] J.D. Zooh, D.W. Burns, H. Guckel, J.J. Sniegowski, R.L. Englstad, Z. Feng, Characteristic of polysilicon resonant microbeams, *Sensors and Actuator A* 35 (1992) 51–59.
[13] M.K. Andrews, P.D. Harris, Damping and viscosity measurements using a microstructure, *Sensors and Actuators A* 49 (1995) 103–108.
[14] P. Kumar, E. Foufoula-Georgiou, Wavelet analysis for geophysical applications, *Reviews of Geophysics* 35 (1997) 385–412.
[15] S. Mallat, *Une exploitation des signaux en ondelettes*, Editions de l'Ecole Polytechnique, Paris, 2000.
[16] M. Ruzzene, A. Fasana, L. Garibaldi, B. Piombo, Natural frequencies and dampings identification using wavelet transform: application to real data, *Mechanical Systems and Signal Processing* 11 (1997) 207–218.
[17] J. Slavic, I. Simonovski, M. Boltezar, Damping identification using a continuous wavelet transform: application to real data, *Journal of Sound and Vibration* 262 (2003) 291–307.

[18] J. Lardies, S. Gouttebroze, Identification of modal parameters using the wavelet transform, *International Journal of Mechanical Sciences* 44 (2002) 2263–2283.
[19] J. Lardies, M.N. Ta, M. Berthillier, Modal parameter estimation based on the wavelet transform of output data, *Archive of Applied Mechanics* 73 (2004) 718–733.
[20] L. Heller, Amortissement Dans les Structures Assemblées, PhD Thesis, University of Franche-Comté, France, 2005.
[21] M. Martarelli, G.M. Revel, C. Santolini, Automated modal analysis by scanning laser vibrometry: problem and uncertainties associated with the scanning system calibration, *Mechanical Systems and Signal Processing* 15 (2001) 581–601.
[22] H. Nouira, L. Heller, E. Foltête, L. Hirsinger, Influence of air pressure on the micro-beam dynamics, *International Modal Analysis Conference*, St. Louis Missouri, USA, February 2006.
[23] M.N. Ta, J. Lardies, Identification of weak non-linearities on damping and stiffness by the continuous wavelet transform, *Journal of Sound and Vibration* 293 (2006) 16–37.
[24] Z. Osinski, *Damping of Vibrations*, A.A. Balkema, Rotterdam, Netherlands, 1998.
[25] S.D. Panteliou, T.G. Chondros, V.C. Argyrakis, Damping factor as an indicator of crack severity, *Journal of Sound and Vibration* 241 (1999) 235–245.
[26] V.T. Srikar, S.D. Senturia, Thermoelastic damping in fine-grained polysilicon flexural beam resonators, *Journal of Microelectromechanical Systems* 11 (2002) 499–504.
[27] A.N. Norris, D.M. Photiadis, Thermoelastic relaxation in elastic structures, with applications to thin plates, *Report, Mechanical and Aerospace Engineering,* Naval Research Laboratory, USA, 2004.
[28] R. Lifshitz, M.L. Roukes, Thermoelastic damping in micro- and nanomechanical systems, *Physical Review B* 61 (2000) 5600–5609.
[29] G.S. Kino, *Acoustic Waves: Devices, Imaging, and Analog Signal Processing*, Prentice-Hall, New Jersey, 1987.
[30] A. Toufine, J.J. Barrau, M. Berthillier, Dynamic study of a structure with flexion-torsion coupling in the presence of dry friction, *Nonlinear Dynamics* 18 (1999) 321–337.
[31] L.E. Goodman, J.H. Klumpp, Analysis of slip damping with reference to turbine-blade vibration, *Journal of Applied Mechanics* (1956) 421–429.
[32] M. Schatzman, C.H. Lamarque, J. Bastien, An ill-posed mechanical problem with friction, *European Journal of Mechanics—A/Solids* 18 (1999) 415–420.
[33] K. Kokubum, M. Hiata, H. Murakami, Y. Toda, M. Ono, A bending and stretching mode crystal oscillator as a friction vacuum gauge, *Vacuum* 34 (1984) 731–735.